Integral Sliding Mode for the Torque-Vectoring Control of Fully Electric Vehicles: Theoretical Design and Experimental Assessment

Tommaso Goggia, Aldo Sorniotti, *Member, IEEE*, Leonardo De Novellis, *Member, IEEE*, Antonella Ferrara, *Senior Member, IEEE*, Patrick Gruber, Johan Theunissen, Dirk Steenbeke, Bernhard Knauder, and Josef Zehetner, *Member, IEEE*

***Abstract*—This paper presents an integral sliding mode (ISM) formulation for the torque-vectoring (TV) control of a fully electric vehicle. The performance of the controller is evaluated in steady-state and transient conditions, including the analysis of the controller performance degradation due to its real-world implementation. This potential issue, which is typical of sliding mode formulations, relates to the actuation delays caused by the drivetrain hardware configuration, signal discretization, and vehicle communication buses, which can provoke chattering and irregular control action. The controller is experimentally assessed on a prototype electric vehicle demonstrator under the worst-case conditions in terms of drivetrain layout and communication delays. The results show a significant enhancement of the controlled vehicle performance during all maneuvers.**

***Index Terms*—Actuation delays, experimental tests, integral sliding mode (ISM), torque-vectoring (TV), yaw rate control.**

NOMENCLATURE

a, b	Front and rear semi-wheel bases.
a_x, a_y	Longitudinal and lateral vehicle accelerations.
c_F, c_R	Front and rear track widths.
c_{hs}, k_{hs}	Half-shaft torsion damping coefficient and torsional stiffness.
f, h, n, k	Known functions of the states (x), the contribution due to uncertainties and disturbances, the term multiplied by the control input, and the yaw acceleration contribution due to lateral tire forces and self-aligning torques (SAT), respectively.
f_r	Tire rolling resistance coefficient.
F_x, F_y, F_z	Longitudinal, lateral, and vertical tire forces, respectively.
G_f	Increment of the motor-torque excitation frequency per unit time in a sweep test.
i	Transmission gear ratio.
J	Moment of inertia of the transmission components (shafts and gears).
J_m, J_{hs}, J_w	Motor, half-shaft, and wheel moments of inertia, respectively.
J_z	Vehicle yaw moment of inertia.
K	Gain of the discontinuous part of the ISM control action.
K_b	Ratio between friction brake torque and friction brake pressure.
K_P, t_I, t_D, t_t	Constants defining the gains of the proportional integral derivative (PID) controller (including anti-windup).
K_U	Understeer gradient.
M_{SAT}	Tire SAT.
M_z, $M_{z,unc}$	Generic yaw moment and yaw moment due to system uncertainties and disturbances, respectively.
M_{z,F_x}	Yaw moment contribution due to longitudinal tire forces.
$M_{z,ISM}$	Output yaw moment of the integral sliding mode (ISM) controller.
$M_{z,PID}$	Yaw moment contribution of the PID controller within the ISM control structure.
$M_{z,sw}$, $M_{z,sw,f}$	Yaw moment contribution due to the switching (discontinuous) part of the ISM and its filtered value (with time derivative $\dot{M}_{z,sw,f}$).
p_{acc}, p_{br}	Accelerator pedal and brake pedal positions, respectively.
p_b, T_b	Friction brake pressure and friction brake torque, respectively.
P_{peak}, T_{peak}	Motor peak power and peak torque, respectively.
r, $\dot{r}$, r_{LUT}	Vehicle yaw rate, yaw acceleration, and reference yaw rate from the look-up table (LUT), respectively.
R_l	Laden wheel radius.

Manuscript received November 3, 2013; revised April 15, 2014; accepted June 26, 2014. Date of publication July 16, 2014; date of current version May 12, 2015. The research leading to these results has received funding from the European Union's Seventh Framework Programme FP7/2007-2013 under grant agreement no. 284708. The review of this paper was coordinated by Prof. J. Wang.

T. Goggia was with the University of Surrey, Guildford GU2 7XH, U.K. He is now with McLaren Automotive Ltd., Woking GU21 4YH, U.K.

A. Sorniotti, L. De Novellis, and P. Gruber are with the University of Surrey, Guildford GU2 7XH, U.K. (e-mail: a.sorniotti@surrey.ac.uk).

A. Ferrara is with the University of Pavia, 27100 Pavia, Italy.

J. Theunissen and D. Steenbeke are with Flanders' Drive, 3920 Lommel, Belgium.

B. Knauder is with the Virtual Vehicle Research Center, 8010 Graz, Austria.

J. Zehetner was with the Virtual Vehicle Research Center, 8010 Graz, Austria. He is now with AVL List GmbH, 8020 Graz, Austria.

Color versions of one or more of the figures in this paper are available online at http://ieeexplore.ieee.org.

Digital Object Identifier 10.1109/TVT.2014.2339401

t	Time.
t_{bit}	Time required to transmit a bit.
t_c	Transmission time in the controller area network (CAN) bus.
$t_{d,Comm}$, $t_{d,Send}$, $t_{d,Trsm}$, $t_{d,Rcv}$	Times corresponding to the total communication delay in the CAN bus, and the time delays to send, transmit, and receive the message, respectively.
t_{jitter}	Time between the initiating event and message being queued.
$t_{man,in}$, $t_{man,fin}$	Initial and final times, respectively, of the relevant part of the maneuver, i.e., part characterized by a steering wheel input.
t_{queue}	Time that the message can remain in the CAN controller slot before transmission is started.
T_{hs}, T_w, T_{w,M_z}	Half-shaft torque, wheel torque, and overall wheel torque output by the yaw moment controller.
T_m, $T_{m,0}$, $T_{m,amp}$	Motor torque, average motor-torque level, and amplitude of the motor-torque sinusoidal oscillation.
u, u_1	ISM control action and its discontinuous part.
v	Vehicle speed.
β	Vehicle sideslip angle.
δ_w, δ_{sw}	Steer angle (at the wheel) and steering-wheel angle, respectively.
η	Efficiency of a transmission component.
σ, σ_0, z	Sliding variable (with time derivative $\dot{\sigma}$), conventional term of the sliding variable, and term of the sliding variable typical of ISM (with time derivative $\dot{z}$), respectively.
ϑ_m, $\dot{\vartheta}_m$, $\ddot{\vartheta}_m$	Motor angular displacement, velocity, and acceleration, respectively.
ϑ_w, $\dot{\vartheta}_w$, $\ddot{\vartheta}_w$	Wheel angular displacement, velocity, and acceleration, respectively.
τ_{ISM}	Time constant of the filter adopted for smoothing the discontinuous part of the ISM.
$\tau_{T,F}$, $\tau_{M,F}$	Front-to-total wheel torque distribution and yaw moment distribution ratios.
μ_x, μ_y, μ	Longitudinal, lateral, and overall tire–road friction coefficients, respectively.
ω_r	Cutoff frequency for the generation of r_{dem}.

Legends and Subscripts

"in-w" and "on-b" (used in the legends of the figures), respectively, indicate in-wheel and on-board drivetrain configurations.

"cont." (used in the legends of the figures) indicates a signal delay model with 0.001 s discretization for all signals and no CAN bus delays.

"discr." (used in the legends of the figures) denotes the discretization values of Table II with the CAN bus delay model.

The subscript "dem" refers to demanded/reference values.

The subscripts "$t1$," "$t2$," and "$t3$" refer to transmission components rotating at different speeds (from the motor to the wheel).

The subscripts "CV1" and "CV2" refer to the inner and outer constant velocity joints, respectively.

The subscripts "$\max$" and "$\min$" refer to the maximum and minimum values of the specified variable or parameter.

The subscripts "1," "2," "3," and "4," respectively, refer to the left front, right front, left rear, and right rear drivetrains. The generic drivetrain is indicated with the subscript "j."

I. Introduction

A. Torque-Vectoring Control

FULLY electric vehicles with individually controlled motors allow a significant improvement in vehicle performance in steady-state and transient cornering conditions [1]–[4]. This can be achieved through the active variation of the wheel torque distribution, commonly referred to as torque-vectoring (TV) control [5]. However, at the moment, there is no general consensus about how to exploit the full potential benefit of TV [6]. In particular, some researchers indicate the possibility of varying the vehicle understeer characteristic in conditions of constant velocity to modify the steering response and make it more linear and sports oriented [7], [8]. Other researchers [9] have demonstrated the significant variation of vehicle understeer for conventional vehicles with even left-to-right torque distribution as a function of the amount of traction or braking forces. This phenomenon can be at least partially compensated by TV [10].

In this paper, the TV controller is designed to track a reference set of understeer characteristics defined for different values of longitudinal vehicle acceleration a_x for two driving modes: 1) a "Normal" driving mode aimed at providing a steady-state vehicle response close to that of a conventional vehicle in conditions of constant velocity and 2) a "Sport" driving mode aimed at extending the linear region of steady-state vehicle response and achieving a higher maximum value of lateral acceleration a_y.

Moreover, the TV controller must reduce vehicle yaw rate oscillations in transient conditions, which can be difficult to accomplish particularly if the steady-state response is tuned to be particularly sports oriented.

TV requires the implementation of a continuously active yaw rate controller for the smooth and precise tracking of a reference yaw rate through the generation of a reference yaw moment. This is beyond the state of the art of the stability control systems currently installed on passenger cars, which intervene through engine torque reduction and friction brakes only when the offset between the reference and actual yaw rates is above the assigned thresholds [11].

B. State-of-the-Art of Yaw Moment Control

Industrial vehicle stability controllers are based on PID control structures with complex multiparametric gain scheduling,

e.g., depending on vehicle speed and the estimated under/oversteer condition. Yaw rate controllers suitable for the continuous generation of the reference yaw moment for a TV system include the combination of PID and feedforward, first- and second-order sliding modes [12], [13], linear quadratic regulators [14], and advanced optimal controllers [15]. However, the problem of the continuous tracking of the reference yaw rate is far from being solved in a conventionally accepted way. The specifications for the ideal controller are 1) being designed with the specific purpose of tracking a set of understeer characteristics significantly different from the one of the passive vehicle, 2) having the required robustness properties (e.g., toward the variation of vehicle parameters), 3) being tested on actual vehicle prototypes, 4) not requiring very extensive experimental tuning procedures, 5) not requiring advanced and precise state observers, and 6) providing sufficient smoothness of the control action. The detailed process for the generation of the reference understeer characteristics is described in [10] and [16].

In particular, among sliding mode controllers, first-order sliding mode control can guarantee absence of significant vibrations of the control action only if its discontinuous output is approximated with a saturation function [12]. However, in this condition, the formulation loses its robustness properties and can be considered equivalent to a saturated high-gain proportional controller [19]. Second-order sliding mode can provide robustness and smooth control yaw moment [13]; however, its performance is significantly affected by the actuation dynamics and signal discretization, which are very relevant factors in the implementation of the control system on an actual vehicle. This crucial point can prevent the industrial adoption of sliding mode control structures for vehicle TV control. A comparison of different feedback control structures for vehicle yaw moment control, including two formulations of second-order sliding mode, is presented in [17]. In [18], sliding mode controllers are coupled with energy-efficient control allocation algorithms for the distribution of the wheel torque demands to achieve a vehicle dynamics-related objective. The overall control structure was experimentally assessed on an electric vehicle prototype.

C. Objectives

This paper presents a yaw moment controller based on ISM [19], [20], which combines robustness, ease of tuning and smooth control action. The objectives are as follows:

- to discuss the yaw moment control formulation based on ISM;
- to analyze the robustness of the ISM control structure against the discrete implementation of the controller, including the delays and dynamics of the actuation system, in particular those caused by an on-board layout of the electric drivetrains;
- to experimentally validate the performance of the ISM controller on a two-wheel-drive electric vehicle demonstrator with on-board drivetrains in steady-state and transient conditions for two driving modes ("Normal" and "Sport").

This paper is organized as follows. Section II discusses the developed simulation models, which are used in Section IV for the assessment of the controller described in Section III. Finally, Section V analyzes the vehicle test results.

II. Vehicle Model

This section describes the simulation models of the chassis, electric drivetrain, and vehicle communication buses. Accurate system modeling is important during the design of sliding mode controllers with respect to chattering prevention and smoothness of control action. Initial simulations and experimental studies proved that yaw moment control based on suboptimal second-order sliding mode (presented in [17]) is characterized by good performance for a limited range of drivetrain parameters and input/output (I/O) signal discretization characteristics. Outside this range, significant chattering and vibrations were experienced (because of the actuation delays), which made the adoption of second-order sliding mode impractical for the specific vehicle prototype investigated here. The performance decay due to discretization did not happen with a conventional controller combining PID and feedforward control actions.

As a consequence, a detailed analysis of the robustness of ISM performance against a wide range of drivetrain parameters (including in-wheel and on-board layouts and signal discretization) is required for assessing the real-world applicability of such a controller.

A. Chassis Model

The development of the control system was carried out on an experimentally validated chassis model, implemented in CarMaker (IPG Automotive), including the coupled dynamics of the sprung and unsprung masses and the nonlinear suspension elastokinematics. Tire steady-state behavior is modeled with Pacejka's Magic Formula (i.e., calculating longitudinal and lateral tire forces and SATs), and tire dynamics are considered with a first-order relaxation length model [21].

B. Drivetrain Model

The electric drivetrains are modeled in MATLAB/Simulink and integrated in the CarMaker simulator, which covers both two-wheel-drive and four-wheel-drive configurations. In particular, two drivetrain layouts are adopted to evaluate the robustness of the ISM controller.

1) The first layout is an in-wheel drivetrain layout, in which the electric motor drives are part of the unsprung masses and are connected to the wheels through an in-wheel single-speed transmission [22]. The absence of half-shafts and constant-velocity joints prevents torsional oscillations, allowing precise wheel torque control. With such a configuration, the drivetrain dynamics are governed by the following equation (the subscript indicating the individual drivetrain is omitted for simplicity):

$$\frac{T_m \eta}{i} - T_b - F_x R_l - f_r F_z R_l = \left(J_w + J + \frac{J_m \eta}{i^2} \right) \ddot{\vartheta}_w \quad (1)$$

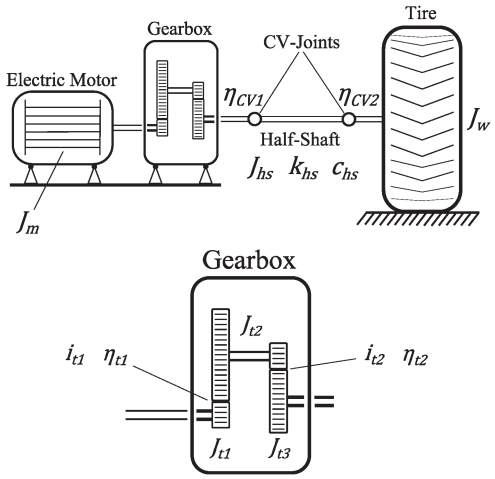

Fig. 1. Schematic of the on-board electric drivetrains.

where T_m is the motor torque; η is the efficiency of the transmission; i is the transmission gear ratio; T_b is the friction brake torque; F_x is the longitudinal tire force; R_l is the laden wheel radius; f_r is the tire rolling resistance coefficient; F_z is the vertical tire force; J_w, J, and J_m are the moments of inertia of the wheel, the transmission, and the motor, respectively; and $\ddot{\vartheta}_w$ is the angular acceleration of the wheel.

2) The second layout is an on-board drivetrain layout (see Fig. 1), which is implemented on a vehicle demonstrator. This drivetrain configuration represents the only feasible option (for packaging reasons) with existing motor technology when high values of peak power are required. In this case, the dynamics of each drivetrain, including a two-stage single-speed transmission, are governed by

$$T_m - \frac{T_{\rm hs} i_{t1} i_{t2}}{\eta_{t1}\eta_{t2}\eta_{\rm CV1}} = \left[J_m + J_{t1} + \frac{i_{t1}^2}{\eta_{t1}} J_{t2} + \frac{i_{t1}^2 i_{t2}^2}{\eta_{t1}\eta_{t2}} \left(J_{t3} + \frac{J_{\rm hs}}{2\eta_{\rm CV1}} \right) \right] \ddot{\vartheta}_m \quad (2)$$

where $T_{\rm hs}$ is the half-shaft torque; i_{t1} and i_{t2} are the gear ratios of the first and second transmission stages, respectively; η_{t1}, η_{t2}, and $\eta_{\rm CV1}$ are the efficiencies of the two transmission stages and the inner constant velocity joint, respectively; J_{t1}, J_{t2}, and J_{t3} are the moments of inertia of the primary, secondary, and output shafts, respectively; and $\ddot{\vartheta}_m$ is the angular acceleration of the motor. The half-shaft torque $T_{\rm hs}$ is given by

$$T_{\rm hs} = c_{\rm hs}(\dot{\vartheta}_m i_{t1} i_{t2} - \dot{\vartheta}_w) + k_{\rm hs}(\vartheta_m i_{t1} i_{t2} - \vartheta_w) \quad (3)$$

where $c_{\rm hs}$ and $k_{\rm hs}$ are the torsion damping coefficient and torsion stiffness of the half-shaft, respectively; ϑ_m and $\dot{\vartheta}_m$ are the angular displacement and velocity of the motor, respectively; and ϑ_w and $\dot{\vartheta}_w$ are the angular displacement and velocity of the wheel, respectively.

The wheel dynamics are expressed by

$$T_w - T_b - F_x R_l - f_r F_z R_l = J_w \ddot{\vartheta}_w. \quad (4)$$

TABLE I
MAIN ON-BOARD DRIVETRAIN PARAMETERS

Symbol	Description	Quantity
P_{peak}	Motor peak power	110 kW
T_{peak}	Motor peak torque	220 Nm
J_m	Motor inertia	0.013 kgm^2
$i_{t1}i_{t2}$	Overall gear ratio	1/10.5
k_{hs}	Torsion stiffness of the half-shaft assembly	12,000 Nm/rad

The drivetrain torque at the wheel T_w is

$$T_w = T_{\rm hs}\eta_{\rm CV2} - \frac{J_{\rm hs}\eta_{\rm CV2}}{2}\ddot{\vartheta}_w \quad (5)$$

where $J_{\rm hs}$ is the moment of inertia of the half-shaft, and $\eta_{\rm CV2}$ is the efficiency of the outer constant velocity joint.

The main parameters of the on-board drivetrains are listed in Table I. The motor performance-related parameters have been obtained through experimental measurements on a test rig of the motor manufacturer. The switched reluctance electric motor drives are characterized by an efficiency map (function of torque and speed), which has significant regions where the motor efficiency is over 90%. The drivetrain data mostly affecting the first natural frequency of the system are J_m (obtained from the CAD model of the component), and $k_{\rm hs}$ (obtained from experimental measurements on the half-shaft assembly, including the constant-velocity joints). Moreover, the frequency response characteristic of the on-board drivetrain varies depending on vehicle speed, motor torque, and tire-slip ratio. The potential impact of the drivetrain dynamics on the vehicle response is experimentally demonstrated in Fig. 2, obtained with the two-wheel-drive electric vehicle prototype used for the ISM experimental tests. Fig. 2 shows the time history of the longitudinal acceleration a_x during sweep tests of the front electric motor torque demands $T_{m,\rm dem}$, which are expressed by

$$T_{m,\rm dem} = T_{m,0} + T_{m,\rm amp}\,\sin(2\pi G_f t^2) \quad (6)$$

with $G_f = 5$ Hz/s, a frequency range starting from 0 Hz, an initial vehicle speed v of 14 m/s, and three combinations of average motor-torque level $T_{m,0}$ and amplitude of the motor torque $T_{m,\rm amp}$.

The noticeable resonance peaks of a_x (approximately between 8 and 10 Hz depending on the test) are induced by the torsional dynamics of the drivetrain. These phenomena can be particularly evident in electric drivetrains because they do not contain a clutch damper as internal-combustion-engine drivetrains. The resonances can cause chattering and vibration in sliding mode controllers. For some electric vehicle applications, specific control schemes have been proposed for the compensation of the on-board drivetrain dynamics including the effect of mechanical backlash [23], [24]. In this activity, such control schemes are not considered in order to show the robustness of the ISM formulation against the actuation system dynamics.

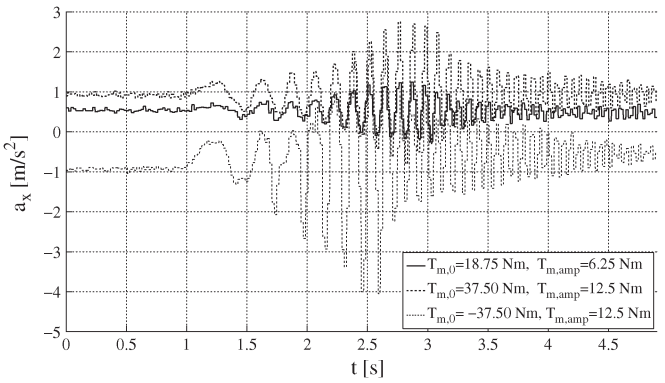

Fig. 2. Impact of the electric drivetrain dynamics on the longitudinal acceleration profile of the vehicle. Experimental results obtained at the Lommel proving ground (Belgium) on the two-wheel-drive electric vehicle prototype adopted for ISM demonstration.

C. Signal Discretization and Delay Model

The vehicle simulator includes the model of the communication delays $t_{d,\mathrm{Comm}}$, experienced in the CAN bus adopted for signal transmission between the control units of the vehicle [25]–[27]. The idea is to augment the system with uncertain terms induced by time-varying delays to show the controller robustness in a similar way as described in [28]. In particular, the communication delays are expressed as the sum of the time delays related to the sending $(t_{d,\mathrm{Send}})$, transmitting $(t_{d,\mathrm{Trsm}})$, and receiving $(t_{d,\mathrm{Rcv}})$ of the message, i.e.,

$$t_{d,\mathrm{Comm}} = t_{d,\mathrm{Send}} + t_{d,\mathrm{Trsm}} + t_{d,\mathrm{Rcv}}. \tag{7}$$

The transmission delay represents the dominant part of $t_{d,\mathrm{Comm}}$. For simplicity, $t_{d,\mathrm{Send}}$ and $t_{d,\mathrm{Rcv}}$ are calculated as constant fractions of $t_{d,\mathrm{Trsm}}$ in the model. In particular, $t_{d,\mathrm{Trsm}}$ consists of the following contributions: 1) the release jitter t_{jitter}, which is the time between the initiating event and the message being queued, ready to be transmitted on the bus; 2) the queuing time t_{queue}, which is the time that the message can remain in the CAN controller slot before transmission is started up; and 3) the transmission time t_c, which is the time that the message takes to be transmitted. Thus, it can be defined as

$$t_{d,\mathrm{Trsm}} = t_{\mathrm{jitter}} + t_{\mathrm{queue}} + t_c. \tag{8}$$

The queuing time includes 1) the blocking time, which is caused by an ongoing transmission process on the data bus, 2) the time that originates from an erroneous message transmission or its repetition, and 3) the transmission time of all messages with higher priority and therefore being sent before the considered message. The detailed formulas adopted within the model (omitted here for brevity) are given in [27].

Within the communication channel model, the transmission delay is uniformly distributed between upper and lower boundaries. Depending on the bus load, this function is shifted toward the worst-case transmission delay for higher bus loads and toward the best-case transmission delay for lower bus loads.

The developed communication channel model has been validated using a CAN bus record from a test vehicle driven in urban and suburban areas. Fig. 3 shows the communication delays of six messages with different priorities extracted from the total 60 messages of the bus traffic. The measured values represent the mean values determined in a measurement range of approximately 17 minutes, during which the bus load varied between 15% and 30%. The best-case and worst-case delays were derived using the model equations. The reference values (center of the probability distribution function) were derived for a bus load of 25%. The graph shows that the model gives a good fit of the measurement data in terms of the communication delay.

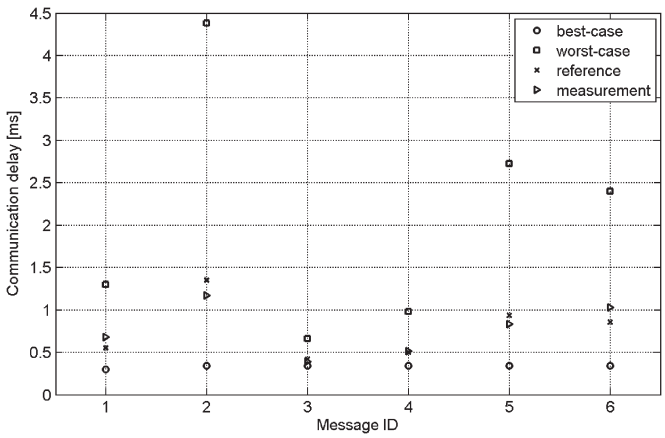

Fig. 3. Experimental validation of the communication channel model.

TABLE II
DISCRETIZATION TIMES AND CAN BUS INTERFACE (YES: PRESENT; NO: ABSENT) FOR THE MAIN I/O SIGNALS OF THE CONTROLLER

Signal	Discretization time [ms]	CAN bus	I/O
δ_{sw}	10	Yes	I
r	10	No	I
a_x	10	No	I
a_y	10	No	I
$\dot{\vartheta}_{w,h}$	2	Yes	I
$T_{m,max,j}$	10	Yes	I
$T_{m,dem,j}$	2	Yes	O
$p_{b,dem,j}$	2	Yes	O

Table II reports the values of the discretization times adopted for the main I/O signals of the controller during the simulations in Section IV and the experimental tests in Section V as well as whether the CAN bus is involved in the transmission of the specific signal. If the time-varying delays of classical message scheduling procedures cause control performance degradation, a dynamic priority scheduling procedure can improve the situation [29]. In the specific application of this paper, which is similar to the setup of current production vehicle implementations of stability control systems, the filtering delay of the sensors (accelerometers, yaw rate sensors, and steering wheel angle sensors designed to provide high dynamic performance) has the same order of magnitude as the communication delays. Discretization affects the sliding mode since the switching frequency is not infinite but finite for digitally implemented sliding modes. Therefore, the sliding motion takes place in a small neighborhood of the sliding manifold, whose dimension is inversely proportional to the control switching frequency. The control signal, commuting at the sampling frequency, provokes

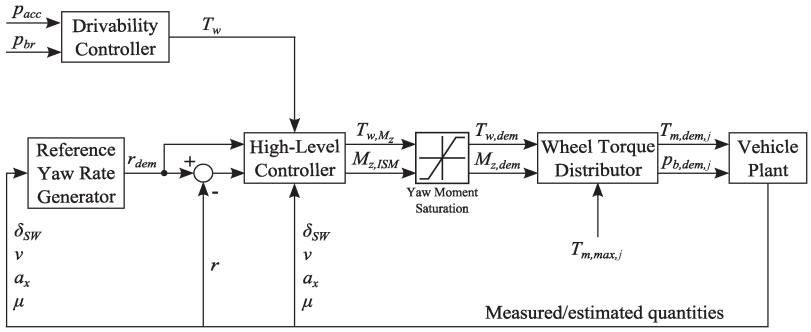

Fig. 4. Simplified schematic of the TV controller.

"ringing," i.e., the chattering effect caused by a piecewise control signal commuting at the sampling frequency between two opposite values.

III. Torque-Vectoring Controller

A. Torque-Vectoring Control Structure

The structure of the TV system is shown in Fig. 4. The drivability controller calculates the reference value of the overall wheel torque T_w based on the driver inputs in terms of accelerator ($p_{\rm acc}$) and brake ($p_{\rm br}$) pedal positions, and the available motor torque. In the reference yaw rate generator, a LUT is included (derived from a reference set of understeer characteristics) to calculate the steady-state reference yaw rate $r_{\rm LUT}$ as a function of the steering wheel angle $\delta_{\rm sw}$, vehicle velocity v, longitudinal acceleration a_x, and road friction condition μ. Using this reference value, the yaw rate reference $r_{\rm dem}$ is calculated with a first-order transfer function such that $r_{\rm dem} = r_{\rm LUT}(\omega_r/(s+\omega_r))$, where ω_r is a cutoff frequency, and s is the Laplace variable. $r_{\rm dem}$ and the actual yaw rate r are sent to the high-level controller, which generates the reference yaw moment $M_{z,\rm ISM}$ to track $r_{\rm dem}$.

Depending on the amount of the yaw rate error $r_{\rm dem} - r$ and its sign (which determines vehicle understeer or oversteer conditions with respect to the reference one), the yaw moment controller can correct T_w; e.g., during traction, T_w is reduced in critical conditions for vehicle safety (for high values of yaw rate error, particularly in the case of vehicle oversteer), thus generating T_{w,M_z} such that $T_{w,M_z} \le T_w$. In general, a reduction of wheel torque allows higher lateral tire forces, and reduces vehicle speed, yielding to lower steady-state values of lateral acceleration and sideslip angle.

$M_{z,\rm ISM}$ and T_{w,M_z} are saturated based on the estimated tire–road friction coefficient (friction estimation is not covered in this paper for brevity; however, useful references are [30]–[33]), and the final yaw moment and wheel torque demands $M_{z,\rm dem}$ and $T_{w,\rm dem}$, respectively, are generated. In particular, the absolute value of the maximum transmissible wheel torque at the drivetrain j is

$$|T_{w,\max,j}| = \mu_{x,j} F_{z,j} R_l \tag{9}$$

where μ_x is the longitudinal friction coefficient.

Hence, the constraints on the demanded wheel torques are

$$\begin{cases} -\left|T_{w,\max,1/2}\right| \le \frac{T_{w,M_z}}{2}\tau_{T,F} \mp \frac{M_{z,\rm ISM}}{c_F}\tau_{M,F}R_l \\ \qquad\qquad \le \left|T_{w,\max,1/2}\right| \\ -\left|T_{w,\max,3/4}\right| \le \frac{T_{w,M_z}}{2}(1-\tau_{T,F}) \\ \qquad\qquad \mp \frac{M_{z,\rm ISM}}{c_R}(1-\tau_{M,F})R_l \le \left|T_{w,\max,3/4}\right|. \end{cases} \tag{10}$$

The subscripts "1," "2," "3," and "4" refer to the left front, right front, left rear and right rear drivetrains, respectively. c_F and c_R are the front and rear track widths, respectively. $\tau_{T,F}$ and $\tau_{M,F}$ are the ratios related to the front-to-total wheel torque and yaw moment distributions, respectively. In a four-wheel-drive vehicle with TV control, $\tau_{T,F}$ and $\tau_{M,F}$ can vary as functions of time and can be based on the minimization of a secondary cost function. Examples of online optimization algorithms are described in [34]–[36]. Owing to the focus on the yaw moment controller of this paper, in traction conditions, $\tau_{T,F} = \tau_{M,F} = 0.5$ is set for the simulated four-wheel-drive vehicles and $\tau_{T,F} = \tau_{M,F} = 1$ for the experimental two-wheel-drive vehicle demonstrator. In braking conditions (which are not considered here), $\tau_{T,F} = \tau_{M,F} = 0.75$, which provides vehicle stability [37]. In the four-wheel-drive vehicles, a smooth transition between the distribution in traction and braking for low values of $|a_x|$ is achieved through a LUT to prevent drivability issues, perceivable by the passengers, during maneuvers characterized by the change of the sign of a_x.

By solving conditions (10), the upper and lower constraints (corresponding to (11) and (12) below) of $M_{z,\rm dem}$ are obtained

$$M_{z,\max} = \min\begin{pmatrix} \frac{c_F}{\tau_{M,F}R_l}\left(\left|T_{w,\max,1/2}\right| \pm \frac{T_{w,M_z}}{2}\tau_{T,F}\right); \\ \frac{c_R}{(1-\tau_{M,F})R_l}\left(\left|T_{w,\max,3/4}\right| \pm \frac{T_{w,M_z}}{2}(1-\tau_{T,F})\right) \end{pmatrix} \tag{11}$$

$$M_{z,\min} = \max\begin{pmatrix} -\frac{c_F}{\tau_{M,F}R_l}\left(\left|T_{w,\max,1/2}\right| \mp \frac{T_{w,M_z}}{2}\tau_{T,F}\right); \\ -\frac{c_R}{(1-\tau_{M,F})R_l}\left(\left|T_{w,\max,3/4}\right| \mp \frac{T_{w,M_z}}{2}(1-\tau_{T,F})\right) \end{pmatrix}. \tag{12}$$

If $M_{z,\max} < M_{z,\min}$, the required wheel torque is greater than the torque permissible by the tire–road friction condition. In this case, (11) and (12) can be rearranged to find the reduced value of wheel torque demand $T_{w,\rm dem}$, meeting the friction

conditions and satisfying $M_{z,\max} \geq M_{z,\min}$. $M_{z,\mathrm{dem}}$ is then obtained through saturation of $M_{z,\mathrm{ISM}}$ as follows:

$$M_{z,\mathrm{dem}} = \mathrm{sat}_{M_{z,\min}}^{M_{z,\max}}(M_{z,\mathrm{ISM}}). \tag{13}$$

Hence, the wheel torque distributor computes the demanded wheel torque providing $M_{z,\mathrm{dem}}$ and $T_{w,\mathrm{dem}}$. At the bottom level, a feedback controller of tire-slip ratio (the detailed description is omitted for brevity) provides the slip control functionality (antilock braking and traction control) and the estimation of the friction coefficients $\mu_{x,j}$. The tire-slip controller intervenes by modifying the wheel torque output by the torque distributor only when the slip ratio exceeds predefined thresholds (beyond which the tire would tend to lock or spin), which is not the case for the simulations and experiments presented in this paper.

From the individual wheel torque demands $T_{w,\mathrm{dem},j}$, the reference motor torques are derived through the following approximation, which considers the motor saturation limits $T_{m,\max,j}$ ($i = i_{t1}i_{t2}$ for on-board drivetrains):

$$T_{m,\mathrm{dem},j} = \min\left(|T_{w,\mathrm{dem},j}|\, i; |T_{m,\max,j}|\right)\mathrm{sign}(T_{w,\mathrm{dem},j}). \tag{14}$$

In case of braking, the friction brakes provide the difference between the demanded torque and the torque achievable through the electric drivetrains. Converting to the friction brake pressure, this difference is given by

$$p_{b,\mathrm{dem},j} = \frac{\frac{T_{m,\mathrm{dem},j}}{i} - T_{w,\mathrm{dem},j}}{K_{b,j}} \tag{15}$$

where K_b is the ratio between the friction brake torque and the friction brake pressure.

B. ISM Controller Formulation

The basic theory of ISM is reported in [19]. The main benefits of ISM over other forms of sliding mode are that 1) ISM starts immediately with sliding motion, without the requirement of the reaching phase during which the system dynamics are not the ideal ones; and 2) ISM can guarantee a smooth control action, without losing its properties, through the first-order filtering of the discontinuous part of its control action. The order of the motion equation with ISM is the same as for the original system. The peculiarity of the ISM formulation is that it shifts the discontinuous control output, typical of sliding mode controllers, from the plant input to the input of an auxiliary dynamic system. As demonstrated in [19], "discontinuity appears only in the internal process; thus, no chattering is excited in the real control path."

ISM must include another control structure to which it provides the robustness properties typical of sliding mode. To demonstrate the effectiveness of ISM, a simple constant-gain PID controller is considered here. On its own, the PID controller would not be able to provide the required tracking performance in steady-state conditions when the reference understeer characteristic is significantly different from the one of the passive vehicle. This shortcoming of the PID is due to the necessary conservativeness in the selection of the gain values, in order to achieve acceptable vehicle stability, transient response and smoothness of control action. From a theoretical viewpoint, ISM is usually considered a perturbation estimator and compensator rather than a controller [19]. However, interestingly, this paper shows that, for the specific application of vehicle yaw moment control, the function of the ISM is well beyond the pure enhancement of robustness. The ISM actually provides a significant control system performance, even when coupled with a controller (the PID) that is unable to guarantee the required yaw rate tracking in nominal conditions.

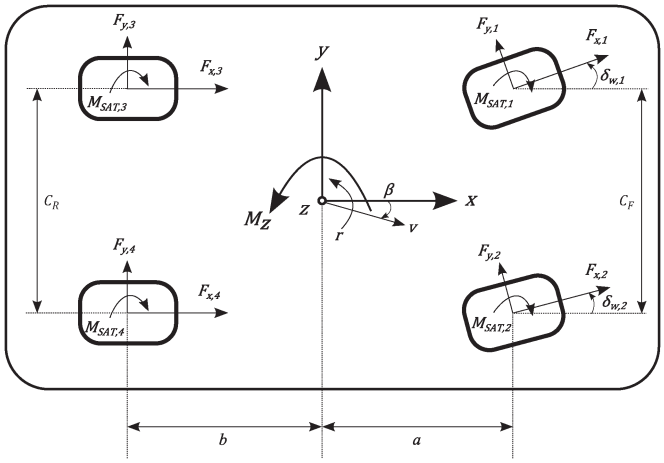

Fig. 5. Top view of the vehicle.

The ISM controller can be developed starting from the yaw moment balance equation of the vehicle (see Fig. 5), i.e.,

$$\begin{aligned} J_z\dot{r} = {} & (-F_{y,2}\sin\delta_{w,2} + F_{y,1}\sin\delta_{w,1} \\ & + F_{x,2}\cos\delta_{w,2} - F_{x,1}\cos\delta_{w,1})\frac{c_F}{2} \\ & + (F_{y,2}\cos\delta_{w,2} + F_{y,1}\cos\delta_{w,1} \\ & + F_{x,2}\sin\delta_{w,2} + F_{x,1}\sin\delta_{w,1})a \\ & - (F_{y,4} + F_{y,3})b + (F_{x,4} - F_{x,3})\frac{c_R}{2} \\ & - M_{\mathrm{SAT},1} - M_{\mathrm{SAT},2} - M_{\mathrm{SAT},3} - M_{\mathrm{SAT},4} \end{aligned} \tag{16}$$

where J_z is the vehicle yaw moment of inertia; F_y is the lateral tire force; δ_w is the steer angle at the wheels; a and b are the front and rear semi-wheelbases, respectively; and M_{SAT} is the tire SAT.

The ISM controller has an impact on the part of the vehicle yaw moment M_{z,F_x}, resulting from longitudinal tire forces $F_{x,j}$, which are directly correlated with the drivetrain torque and friction brake pressures, as described in the following:

$$\begin{aligned} M_{z,F_x} = {} & (F_{x,2}\cos\delta_{w,2} - F_{x,1}\cos\delta_{w,1})\frac{c_F}{2} \\ & + (F_{x,2}\sin\delta_{w,2} + F_{x,1}\sin\delta_{w,1})a + (F_{x,4} - F_{x,3})\frac{c_R}{2}. \end{aligned} \tag{17}$$

The remaining portion of yaw moment is given by the contribution $J_z k$ due to the lateral tire forces and the SATs, i.e.,

$$\begin{aligned} k(r,\beta,\delta_{w,j}) = \frac{1}{J_z}\Big[& (-F_{y,2}\sin\delta_{w,2} + F_{y,1}\sin\delta_{w,1})\frac{c_F}{2} \\ & + (F_{y,2}\cos\delta_{w,2} + F_{y,1}\cos\delta_{w,1})a \\ & - (F_{y,4} + F_{y,3})b - M_{\mathrm{SAT},1} - M_{\mathrm{SAT},2} \\ & - M_{\mathrm{SAT},3} - M_{\mathrm{SAT},4}\Big]. \end{aligned} \tag{18}$$

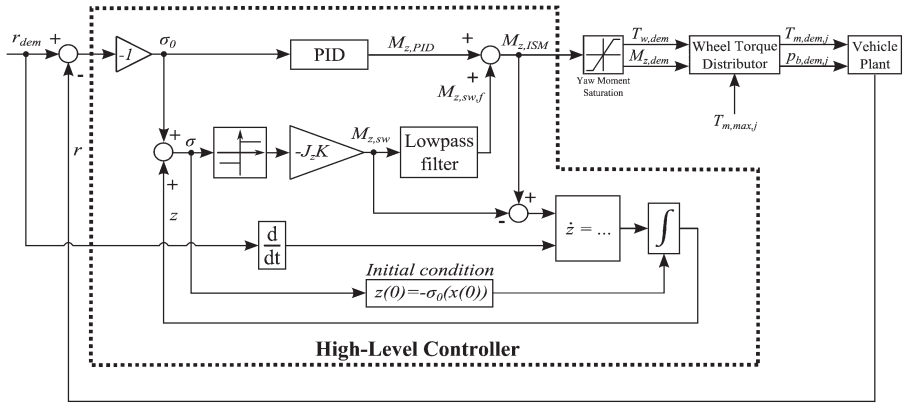

Fig. 6. Simplified schematic of the ISM controller.

Primarily, k is a function of r, β, and $\delta_{w,j}$; tire-slip ratio has a secondary influence on k because of the tire friction ellipse [38]. The yaw acceleration error $\dot{r} - \dot{r}_{\rm dem}$ is obtained by combining (16)–(18) and including the yaw moment contribution due to disturbances and uncertainties $M_{z,\rm unc}$ as follows:

$$\dot{r} - \dot{r}_{\rm dem} = k(r, \beta, \delta_{w,h}) - \dot{r}_{\rm dem} + \frac{1}{J_z} M_{z,F_x} + \frac{1}{J_z} M_{z,\rm unc}. \quad (19)$$

The block diagram of the specific ISM formulation is shown in Fig. 6.

If no form of state estimator is included in the controller (as shown here to demonstrate the robustness of ISM), the uncertain part of (19) is given by $h = k(r, \beta, \delta_{w,j}) + (1/J_z) M_{z,\rm unc}$, and the known part is $f = -\dot{r}_{\rm dem}$. By neglecting the actuation dynamics and the saturation processes within the controller (described in Section III-A), $M_{z,F_x} \cong M_{z,\rm ISM}$, which is given by

$$M_{z,\rm ISM} = M_{z,\rm PID} + M_{z,{\rm sw},f} \quad (20)$$

where the yaw moment contribution of the PID controller is

$$M_{z,\rm PID} = K_P \left(-\sigma_0(t) - \frac{1}{t_I} \int \sigma_0(t) - t_D \dot{\sigma}(t) \right) + \frac{1}{t_t} \int \left(M_{z,\rm dem}(t) - M_{z,\rm ISM}(t) \right) dt. \quad (21)$$

K_P, t_I, and t_D are the parameters of the proportional, integral, and derivative parts of the PID controller, respectively, and σ_0 is the conventional term of the ISM sliding variable as described in the following. To account for nonlinearities due to the saturation of the control action, the PID formulation includes an anti-windup scheme with tuning parameter t_t.

To prevent chattering (i.e., oscillation of the sliding variable) and to eliminate the discontinuity in the control action, the discontinuous part of the control action $M_{z,\rm sw}$ is filtered $(M_{z,{\rm sw},f})$ using the time constant $\tau_{\rm ISM}$ as follows:

$$\dot{M}_{z,{\rm sw},f} \tau_{\rm ISM} + M_{z,{\rm sw},f} = M_{z,\rm sw} \quad (22)$$

with $M_{z,\rm sw}$ being

$$M_{z,\rm sw} = -J_z K \, \text{sign}(\sigma), \quad \text{with } K > |h_{\max}| \quad (23)$$

where K is the controller gain. σ consists of two contributions, which are summed together: 1) σ_0, which corresponds to the usual definition of the sliding variable and depends on the state variables x of the system (here $\sigma_0 = r - r_{\rm dem}$); and 2) z, which is the auxiliary variable (as mentioned in the introduction to ISM) typical of ISM. In particular, its general formulation is [19]

$$\dot{z} = -\frac{d\sigma_0}{dx} \left[f(x) + n(x)u - n(x)u_1 \right] \quad \text{with } z(0) = -\sigma_0(x(0)) \quad (24)$$

where f and n are functions of the states, and u and u_1 are, repectively, the ISM control action and its discontinuous part.

Considering the formulation (19), $\dot{z}$ becomes

$$\dot{z} = -\frac{d\sigma_0}{d(r - r_{\rm dem})} \left[-\dot{r} + \frac{1}{J_z} (M_{z,\rm ISM} - M_{z,\rm sw}) \right] = \dot{r}_{\rm dem} - \frac{1}{J_z} (M_{z,\rm ISM} - M_{z,\rm sw}). \quad (25)$$

The inequality condition in (23) $(K > |h_{\max}|)$ derives from the requirement of an asymptotic stability through the Lyapunov function $V(s) = (1/2)\sigma^2$ since $\dot{\sigma} = \dot{r} - (1/J_z)(M_{z,\rm ISM} - M_{z,\rm sw}) = h + M_{z,\rm sw}/J_z$.

C. Tuning of the ISM Controller Parameters

The tuning of the parameters of the ISM controller must be carried out with the following three objectives:

1) to provide the asymptotic stability of the system according to condition (23);
2) to prevent any form of chattering, which affects the tracking performance of the control system [39], [40];
3) to prevent discontinuity or vibration of the control action. (Ideal sliding mode is characterized by discontinuous control action switching at infinite frequency, without chattering. However, this ideal performance is not suitable for a continuously active TV system, which requires smoothness of the control action for comfort reasons.)

Objective 1 can be achieved through the tuning of K. Appropriate values of K can be derived from the analysis of $h(t)$ for the controlled vehicle in extreme operating conditions or when disturbances or variations of vehicle parameters are introduced. For example, Fig. 7 plots $J_z h(t)$ during a sequence of step steer maneuvers with nominal vehicle parameters and $M_{z,\rm unc} = 0$. This test indicates that a minimum value of 8000 Nm is required

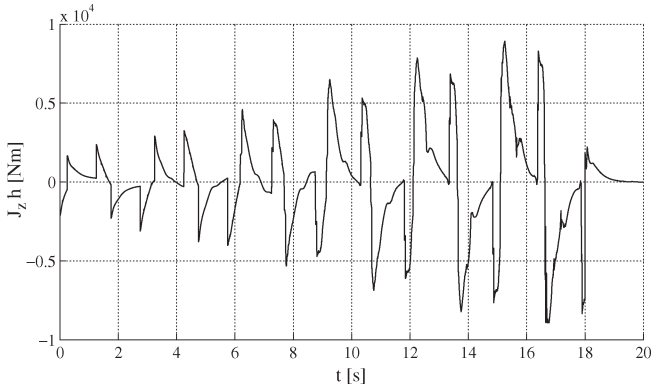

Fig. 7. $J_z h(t)$ during a sequence of step steers for the controlled vehicle.

TABLE III
VALUES OF $\tau_{\rm ISM}$ [S] ADOPTED FOR THE ISM IN THE DIFFERENT DRIVETRAIN CONFIGURATIONS ("IN-WHEEL" AND "ON-BOARD") AND EXCLUDING/INCLUDING THE CAN BUS AND SIGNAL DISCRETIZATION MODEL

	0.001 s discretization w/o CAN	Including discretization and CAN
In-Wheel	0.05	0.30
On-Board	0.50	0.50

for $J_z K$. Nonetheless, to account for a worst-case scenario, all maneuvers reported here (simulated or experimental) are conducted with $J_z K = 15\,000$ Nm. This condition provides control system robustness even without estimation of the lateral tire forces and SATs. Gain scheduling of K depending on v and $\delta_{\rm sw}$ is not discussed in this paper but can be used to ensure system stability during extreme transient conditions and to increase smoothness of the control action at low lateral acceleration levels.

Objectives 2 and 3 are fulfilled through tuning of $\tau_{\rm ISM}$. Larger values of $\tau_{\rm ISM}$ are required in the case of slow actuation system dynamics, as shown in Table III.

IV. EFFECT OF THE ACTUATION SYSTEM DYNAMICS ON THE CONTROL SYSTEM PERFORMANCE

The effect of the actuation system dynamics and I/O signal delays and discretization is evaluated with the model of the four-wheel-drive sports utility electric vehicle described in Section II. In particular, two maneuvers, i.e., ramp steer and sequence of step steers, are simulated.

- Ramp steer consists of a slow rotation of the steering wheel ($\dot{\delta}_{\rm sw} = 10$ deg/s) at $v = 90$ km/h. This maneuver defines the steady-state vehicle response (as the input varies very slowly) through the understeer characteristic. The execution of the ramp steer at constant velocity implies a progressive increase in driver torque demand to compensate the effect of tire-slip power losses. To account for this effect, a feedforward/feedback driver model is included in the simulator. The feedforward contribution generates a wheel torque demand corresponding to the aerodynamic drag losses, rolling resistance losses, inertial losses, and steady-state lateral slip power losses. These losses are estimated starting from the reference speed profile and the actual value of steering wheel angle. The feedback contribution of the driver model includes a PID controller, based on the error between the reference and actual speed profiles for the specific test.
- The sequence of step steers consists of a series of fast rotations of the steering wheel (leftward and rightward), with progressively increasing amplitude (from 30 deg to 130 deg), at $v = 90$ km/h (which implies an increase in driver torque demand when the vehicle is cornering). The successive application of the steering wheel inputs at a frequency close to the natural one of the yaw motion excites the vehicle yaw dynamics, with significant oscillations in the last part of the maneuver. The final steering wheel angle (130 deg) is well above the value required for achieving the maximum lateral acceleration in high friction conditions at 90 km/h.

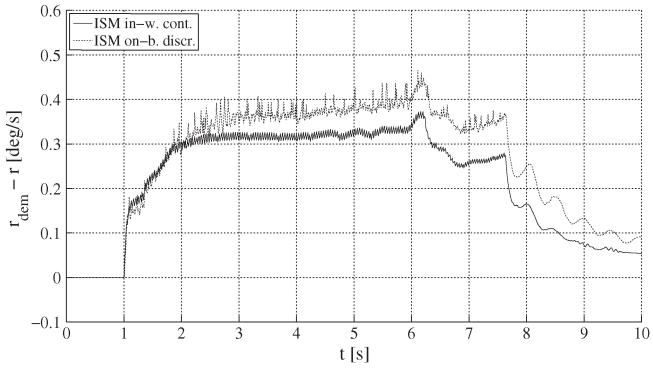

Fig. 8. Yaw rate error as a function of time during a ramp steer maneuver with $\mu = 1$ for in-wheel "in-w" and on-board "on-b" drivetrain configurations; "cont." indicates a signal delay model with 0.001s discretization for all signals and no CAN bus delays, and "discr." denotes the discretization values of Table II with the CAN bus delay model. The same notations will be used in the following figures of the paper.

The simulations are performed with the driving mode set to "Sport," which is the most critical one in terms of steady-state and transient tracking performance. The aim of the analysis is to demonstrate that a simple ISM formulation, not taking into consideration actuation delays, performs well even when significant delays (including time-variant delays), signal discretization, and actuation dynamics are present in the system.

A. Ramp Steer

Fig. 8 shows the yaw rate error $r_{\rm dem} - r$ during the ramp steer maneuver for a sample of the different drivetrain layouts. Only a very small difference can be observed between the configurations, which is considered negligible for this paper.

The tracking performance of the controller is evaluated through the RMSE (root-mean-square error) value of the yaw rate during the part of the maneuver characterized by a steering wheel input, i.e.,

$$\text{RMSE} = \sqrt{\frac{1}{t_{\rm man,fin} - t_{\rm man,in}} \int_{t_{\rm man,in}}^{t_{\rm man,fin}} \left(r_{\rm dem}(t) - r(t)\right)^2 dt} \tag{26}$$

where $t_{\rm man,in}$ and $t_{\rm man,fin}$ are the initial and final times of the relevant part of the maneuver, respectively.

TABLE IV
RMSE VALUES [DEG/S] FOR THE DIFFERENT DRIVETRAIN LAYOUTS AND MESSAGE DELAY OPTIONS DURING THE RAMP STEER MANEUVER, WITH $\mu = 1$

	0.001 s discretization w/o CAN	Including discretization and CAN
In-Wheel	Baseline: 2.792 ISM: 0.249	Baseline: 2.709 ISM 0.265
On-Board	Baseline: 2.791 ISM: 0.296	Baseline: 2.709 ISM: 0.297

TABLE V
$\text{IACA}_{M_{z,\text{dem}}}$ VALUES [Nm] FOR THE DIFFERENT DRIVETRAIN LAYOUTS AND MESSAGE DELAY OPTIONS DURING THE RAMP STEER MANEUVER, WITH $\mu = 1$

	0.001 s discretization w/o CAN	Including discretization and CAN
In-Wheel	1,121	1,100
On-Board	1,154	1,139

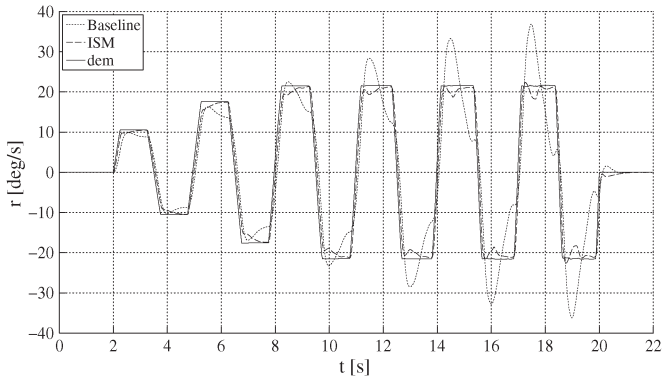

Fig. 9. Reference yaw rate ("dem") and actual yaw rate ("ISM") for the controlled vehicle (in-wheel motors, excluding discretization and CAN delays) and yaw rate of the passive vehicle ("Baseline") during a sequence of step steers, with $\mu = 1$.

The amount of control effort demand is measured by the $\text{IACA}_{M_{z,\text{dem}}}$, i.e., the integral of the absolute value of the control action along the relevant part of the maneuver described as follows:

$$\text{IACA}_{M_{z,\text{dem}}} = \frac{1}{t_{\text{man,fin}} - t_{\text{man,in}}} \int_{t_{\text{man,in}}}^{t_{\text{man,fin}}} |M_{z,\text{dem}}(t)|\, dt. \quad (27)$$

The values of the two indicators are reported in Tables IV and V. The RMSE values for the controlled vehicle are within 10% of the values for the passive ("Baseline") vehicle. Discontinuities or vibrations of the control actions are not observed, and the values of the $\text{IACA}_{M_{z,\text{dem}}}$ are very similar for all the layouts, due to the slow nature of the specific maneuver. Hence, the developed control formulations can be assumed to provide sufficient robustness against actuation system configuration.

B. Sequence of Step Steers

Fig. 9 highlights the benefit deriving from the adoption of the ISM TV controller. For the in-wheel drivetrain configuration without signal delays, the ISM TV controller eliminates the yaw rate overshoots. In the same test, the passive vehicle ("Baseline") reaches a safety-critical yaw rate ($|r|$) value of 37 deg/s (compared with a reference value range of 21–22 deg/s) after the last steering application.

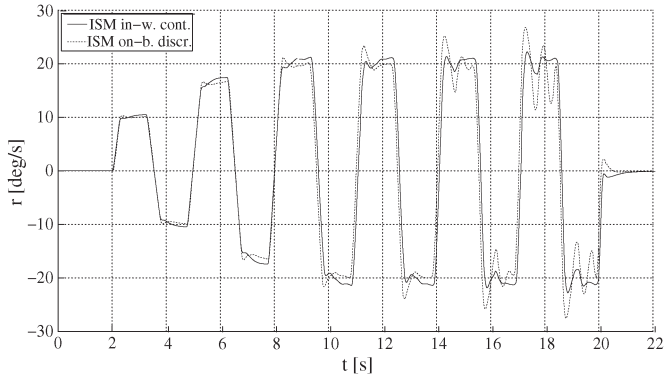

Fig. 10. $r(t)$ for the vehicles with the "in-w. cont." and "on-b. discr." drivetrain configurations, with $\mu = 1$.

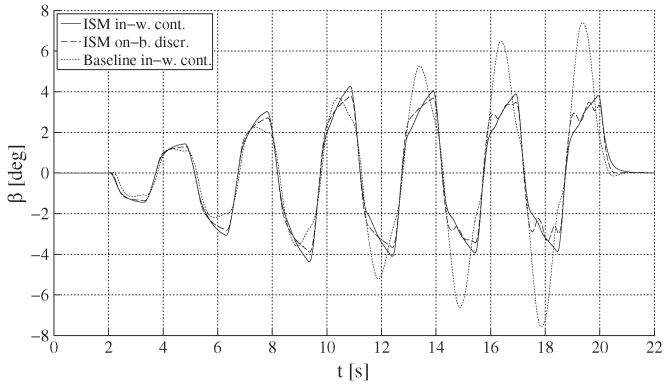

Fig. 11. $\beta(t)$ for the passive vehicle "Baseline" and the vehicles with the "in-w. cont." and "on-b. discr." drivetrain configurations, with $\mu = 1$.

TABLE VI
RMSE VALUES [DEG/S] FOR THE DIFFERENT DRIVETRAIN LAYOUTS AND MESSAGE DELAY OPTIONS DURING A SEQUENCE OF STEP STEERS, WITH $\mu = 1$

	0.001 s discretization w/o CAN	Including discretization and CAN
In-Wheel	Baseline: 6.390 ISM: 2.421	Baseline: 6.277 ISM: 2.678
On-Board	Baseline: 6.393 ISM: 2.658	Baseline: 6.286 ISM: 2.937

The performance decay of the controller related to the different drivetrain layouts is evident (see Figs. 10 and 11), but even the least performing controlled vehicle configuration ("on-b. discr.") exhibits a maximum $|r|$ (i.e., approximately 27 deg/s) that is significantly smaller than with the passive vehicle. Also, the maximum sideslip angle remains below 4 deg with the TV-controlled vehicles, compared with nearly 8 deg for the passive vehicle.

The RMSE values for the controlled vehicle (see Table VI) range between 2.4 and 2.9 deg/s, which is considerably lower than the minimum RMSE value computed for the passive vehicle (at least 6.2 deg/s). Due to actuation bandwidth limitations, the progressive decay of the performance of the actuation system is noticeable during the last couple of steering wheel

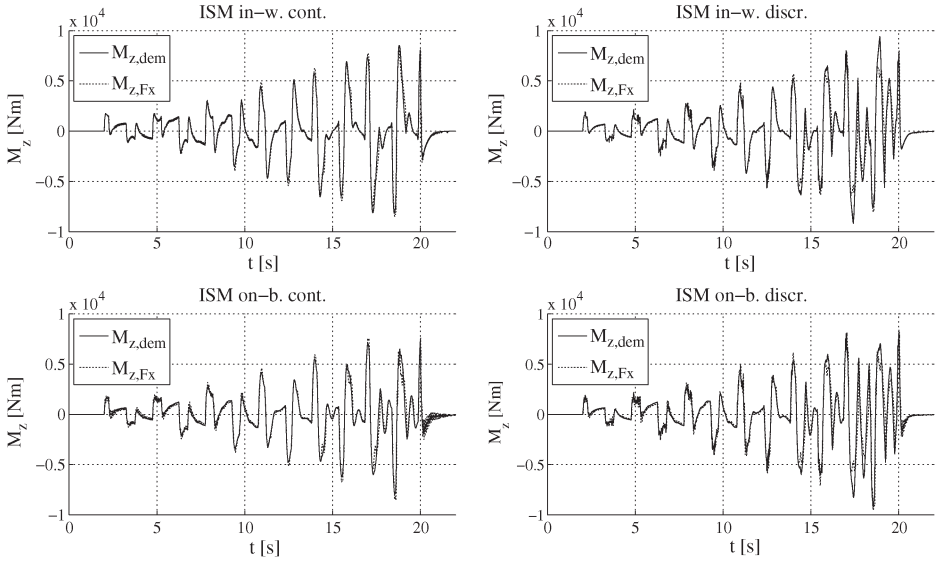

Fig. 12. $M_{z,\mathrm{dem}}(t)$ and $M_{z,F_x}(t)$ for the four different actuation systems (in-wheel and on-board drivetrains including and excluding signal discretization and CAN delays) during a sequence of step steers, with $\mu = 1$.

TABLE VII
IACA VALUES [Nm] FOR THE DIFFERENT DRIVETRAIN LAYOUTS AND MESSAGE DELAY OPTIONS DURING A SEQUENCE OF STEP STEERS, WITH $\mu = 1$

	0.001 s discretization w/o CAN	Including discretization and CAN
In-Wheel	$IACA_{M_{z,dem}} = 1{,}460$ $IACA_{M_{z,F_x}} = 1{,}483$	$IACA_{M_{z,dem}} = 1{,}542$ $IACA_{M_{z,F_x}} = 1{,}507$
On-Board	$IACA_{M_{z,dem}} = 1{,}366$ $IACA_{M_{z,F_x}} = 1{,}348$	$IACA_{M_{z,dem}} = 1{,}581$ $IACA_{M_{z,F_x}} = 1{,}511$

inputs, which provoke a significant amount of oscillations of $M_{z,\mathrm{dem}}$ (see Fig. 12). Although no saturation issues of the control action are experienced during the extreme tests, yaw moment saturation could be required at higher vehicle speeds or for cornering maneuvers at nonzero a_x.

The IACA values (see Table VII, including the index $\mathrm{IACA}_{M_{z,F_x}}$, based on M_{z,F_x}, which is the generated control action) show that the requested control effort changes marginally when signal delays are considered (up to about 200 Nm). This variation is even lower for the actual control effort (up to about 150 Nm). However, when considering the following index:

$$\mathrm{IACA}_{M_{z,\mathrm{dem}}-M_{z,F_x}} = \frac{1}{t_{\mathrm{man,fin}}-t_{\mathrm{man,in}}} \int_{t_{\mathrm{man,in}}}^{t_{\mathrm{man,fin}}} |(M_{z,\mathrm{dem}}(t)-M_{z,F_x}(t))|\,dt \quad (28)$$

which assesses the amount of actuation error, a significant influence of the signal discretization and CAN delays can be observed. As indicated by Table VIII, values of $\mathrm{IACA}_{M_{z,\mathrm{dem}}-M_{z,F_x}}$ of about 400 Nm occur in the worst-case scenario. Even if the RMSE value of the yaw rate tracking performance remains very good, the observed influence of signal discretization and delays justifies the adoption of advanced wheel torque control techniques (e.g., in [23] and [24]) for the improvement of the drivetrain dynamic performance and actuation precision.

TABLE VIII
$\mathrm{IACA}_{M_{z,dem}-M_{z,F_x}}$ [Nm] FOR THE DIFFERENT DRIVETRAIN LAYOUTS AND MESSAGE DELAY OPTIONS DURING A SEQUENCE OF STEP STEERS, WITH $\mu = 1$

	0.001 s discretization w/o CAN	Including discretization and CAN
In-Wheel	215	348
On-Board	276	423

Fig. 13 confirms the excellent performance of the ISM controller in low friction conditions (friction coefficient μ is equal to 0.5), identified by the friction estimator (thus provoking a variation of the yaw rate demand). The tuning parameters (but not the reference yaw rate) of the ISM controller in low friction conditions are the same as for the high friction simulations, to demonstrate the robustness of the control structure.

The passive vehicle is not capable of following the sequence of steering wheel inputs as it is evident from the time histories of $r(t)$ and $\beta(t)$ after 10 s, with values of sideslip angle close to 20 deg (condition of vehicle spin). Table IX reports the values of the RMSE for the different drivetrain layouts, during the same maneuver. The yaw rate tracking performance for $\mu = 0.5$ is even better than the one shown in Table VI for $\mu = 1$ as the tuning of the reference yaw rate in low friction conditions is deliberately less aggressive than for high friction operation because of safety reasons.

V. EXPERIMENTAL RESULTS ON A FULLY ELECTRIC VEHICLE DEMONSTRATOR

A. Vehicle Demonstrator Testing

The prototype on-board electric drivetrains described in Section II were installed at the front axle of a 2011 Range Rover Evoque, and experimental tests were performed at the Lommel proving ground in Belgium under dry road surface conditions (see Fig. 14). In particular, two maneuvers are investigated here.

1) Skid pad test (see Section V-B), in which the vehicle travels along a circular trajectory (30 m radius) at slowly

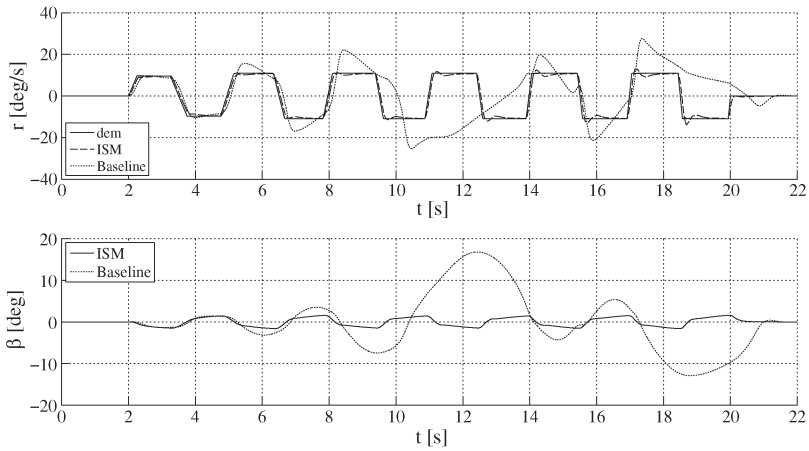

Fig. 13. $r(t)$ and $\beta(t)$ for the controlled vehicle (in-wheel motors, excluding discretization and CAN delays) and the passive vehicle ("Baseline") during a sequence of step steers, with $\mu = 0.5$.

TABLE IX
RMSE VALUES [DEG/S] FOR THE DIFFERENT DRIVETRAIN LAYOUTS AND MESSAGE DELAY OPTIONS DURING A SEQUENCE OF STEP STEERS, WITH $\mu = 0.5$

	0.001 s discretization w/o CAN	Including discretization and CAN
In-Wheel	Baseline: 10.948 ISM: 1.451	Baseline: 12.945 ISM: 1.642
On-Board	Baseline: 12.288 ISM: 1.811	Baseline: 12.317 ISM: 1.819

Fig. 14. Two-wheel-drive electric vehicle demonstrator during an experimental test.

increasing vehicle speed. Steering wheel angle $\delta_{\rm sw}$ is progressively corrected by the driver to follow the reference trajectory. This procedure allows the derivation of the vehicle understeer characteristic $\delta_{\rm sw}(a_y)$.

2) Step steer test (see Section V-C), consisting of a quick application ($\dot{\delta}_{\rm sw} \cong 400$ deg/s) of a steering wheel input with an amplitude of 150°, which is then kept constant until the completion of the maneuver. The final value of the steering wheel angle was selected to ensure that the vehicle is operating at its cornering limit. The vehicle inputs a constant wheel torque demand during the test, equal to the value required to keep vehicle speed v at the initial value (about 50 km/h in this case) in straight ahead conditions. To do so, the accelerator pedal position of the driver is bypassed during the test. Due to the lateral slip losses of the tires, v decreases after the steering wheel input is applied.

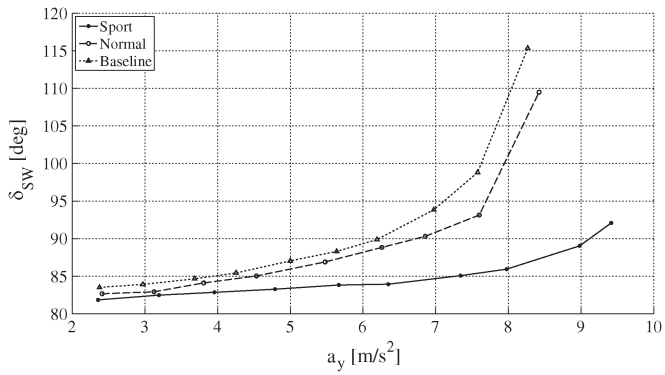

Fig. 15. Experimental understeer characteristics for the passive vehicle ("Baseline") and the active vehicle in "Sport" and "Normal" driving modes.

The values of the discretization step of the different signals, including the specification of the I/O variables transmitted through the CAN bus, are indicated in Table II. The ISM controller was run at a fixed step size of 2 ms on a dSPACE MicroAutoBox system.

B. Skid-Pad Test

Fig. 15 shows the comparison of the experimental understeer characteristics for the "Normal" and "Sport" driving modes of the controlled vehicle and the passive vehicle (symmetric torque distribution on the front axle). The steady-state vehicle response can be significantly modified by the ISM TV controller, which is used to define vehicle handling response according to the driving mode selected by the user. The ISM controller has a major impact on the following three indicators.

- The first indicator is the understeer gradient $K_U = (\partial \delta_{\rm sw})/(\partial a_y)$ at low-to-medium values of lateral acceleration, which for the specific test is about 1 deg $\rm s^2/m$ for the "Baseline" vehicle and the "Normal" driving mode, and 0.6 deg $\rm s^2/m$ for the "Sport" driving mode, between 2.5 and 4 $\rm m/s^2$ of lateral acceleration. This has a direct influence on driver's perception of vehicle response in common driving conditions.
- The second indicator is the extension of the linear region of the vehicle understeer characteristic. The "Baseline"

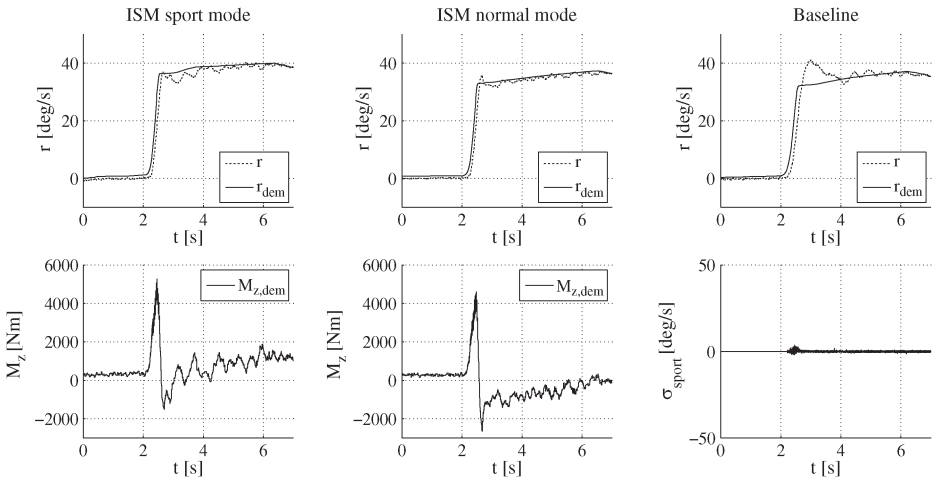

Fig. 16. Experimental results during a step steer maneuver, with a final value of $\delta_{\rm sw}$ of 150 deg, at $v = 50$ km/h.

vehicle and the "Normal" driving mode are characterized by a significant increase in the understeer gradient for medium values of a_y. In fact, K_U is about 2 deg s^2/m for both cases between 4 and 6 m/s^2, doubled from its value between 2.5 and 4 m/s^2. The "Sport" driving mode is characterized by a largely constant value of K_U up to 6–7 m/s^2, which provides a feel of consistent vehicle responsiveness to the driver, even at medium-to-high values of a_y. In any case, above a lateral acceleration threshold, the nonlinearity of the understeer characteristic is required as a safety warning for the driver that the vehicle is close to its cornering limit.

- The third indicator is the increase in the maximum value of lateral acceleration $a_{y,\max}$, which is about 8.3, 8.5, and 9.5 m/s^2, respectively, for the "Baseline" vehicle, the "Normal" driving mode, and "Sport" driving mode, respectively. The increased values of $a_{y,\max}$ denote an improved vehicle handling performance in limit conditions, which are beyond the experience of common drivers. This also means that the controlled vehicle provides additional safety margin during emergency transient maneuvers as it can corner at higher vehicle velocities than the conventional vehicle.

C. Step Steer Test

Fig. 16 compares the performance of the passive vehicle and the ISM-controlled vehicle during the step steer maneuver. In the figure, the yaw rate response of the passive vehicle is overlapped with the reference yaw rate $r_{\rm dem}$ for the "Normal" driving mode, calculated by inputting the time history of the measured variables of the passive vehicle into the controller. The passive vehicle ("Baseline") is characterized by a yaw rate response similar to the one of an underdamped second-order system. The TV controller allows the following benefits with respect to the passive vehicle.

- Considerable reduction in the yaw rate overshoot that follows the application of the steering wheel input. This is critical to vehicle safety. In particular, in the "Sport" mode, the overshoot is eliminated and r peaks at about 37 deg/s (with an overshoot of 1.6% relative to $r_{\rm dem}$).

TABLE X
TIME DELAY [S] BETWEEN $r_{\rm dem}$ AND r (FOR $r_{\rm dem}$ EQUAL TO 15 deg/s AND 30 deg/s) DURING THE STEP STEER MANEUVER OF FIG. 16

	r_{dem} = 15 deg/s	r_{dem} = 30 deg/s
Baseline	0.125	0.136
ISM Normal	0.075	0.080
ISM Sport	0.072	0.078

In the "Normal" mode, the maximum yaw rate is about 36 deg/s (with an overshoot of 8.8%), and the passive vehicle experiences a yaw rate peak of > 41 deg/s (with an overshoot of 26.5%). The reduction of the yaw rate overshoot is achieved by the negative peaks of $M_{z,\rm dem}$ visible in the bottom plots of Fig. 16.

- Decrease in the delay in the initial yaw rate generation, during the application of the steering wheel input. This objective is achieved through the application of a significant $M_{z,\rm dem} > 0$ during the first part of the maneuver. Table X shows a 40% reduction of the time delay between $r_{\rm dem}$ and r. In the specific tuning of the controller, the first-order transfer function for the generation of $r_{\rm dem}$ was removed, to provide a significant increase in vehicle responsiveness and verify the controller stabilization properties in extreme conditions. This justifies the significant peaks of destabilizing $M_{z,\rm dem}$ during the steering wheel application. The introduction of the cutoff frequency ω_r in the reference yaw rate generator (as discussed in Section III) would decrease control aggressiveness during the initial part of the maneuver and further reduce the overshoot.
- Quick stabilization of the system around $r_{\rm dem}$ once the initial transient is completed. In this respect, the controlled vehicle shows a particularly good performance in the "Normal" driving mode.

The ISM sliding variable, reported for the experimental test in the "Sport" mode ($\sigma_{\rm sport}$ in Fig. 16), shows a correct behavior with low amplitude oscillations, which cannot be considered chattering with respect to the nature of the specific physical system. Moreover, in line with theory [19], sliding mode occurs from the start of the maneuver.

VI. Conclusion

A torque-vectoring controller based on integral sliding mode has been presented in this paper. The results lead to the following conclusions.

- The ISM controller achieves a good tracking performance of the reference yaw rate in steady-state and transient conditions, with a smooth control action. This was demonstrated along four maneuvers, involving simulations and experimental tests at different vehicle velocities.
- The continuous part of the implemented ISM controller consists of a PID controller. The performance of the ISM controller is good even when the feedforward contribution (typical of continuously active TV systems) is not included in the continuous part of the ISM formulation. This control structure can significantly reduce the tuning time of the controller compared with conventional formulations.
- The same ISM control structure is compatible with in-wheel and on-board two-wheel-drive and four-wheel-drive layouts and a reasonable range of discretization values and delays of the I/O signals, provided that the time constant τ_{ISM} of the ISM filter is retuned for each system configuration. The same value of the gain K of the discontinuous part of the ISM controller allows good yaw rate tracking performance for all the simulated and experimentally tested maneuvers and drivetrain layouts, even with a large error for the actuation system (measured by the index $\mathrm{IACA}_{M_{z,\mathrm{dem}}-M_{z,F_x}}$).
- The prototype vehicle confirmed the very good functionality of the controller in the worst operational scenario, i.e., on-board electric drivetrains with significant I/O signal discretization and CAN bus delays. The experiments demonstrate the impact TV control can bring in designing steady-state and transient vehicle responses.
- As state estimation is not required, the presented ISM formulation provides ease of tuning, which is important for real world application of the control structure.
- The effect of signal discretization and time delays in the controller I/O signals can be prevalent over the effect of the drivetrain actuation dynamics, in provoking a marginal decay of the tracking performance of the yaw moment controller and increase in the demanded control effort.

References

[1] M. Shino and M. Nagai, "Yaw-moment control of electric vehicle for improving handling and stability," *JSAE Rev.*, vol. 22, no. 4, pp. 473–480, Oct. 2001.

[2] B. Tabbache, A. Kheloui, and M. El Benbouzid, "An adaptive electric differential for electric vehicles motion stabilization," *IEEE Trans. Veh. Technol.*, vol. 60, no. 1, pp. 104–110, Jan. 2011.

[3] C. Ceng, L. Mostefai, M. Denai, and Y. Hori, "Direct yaw-moment control of an in-wheel-motored electric vehicle based on body slip angle fuzzy observer," *IEEE Trans. Ind. Electron.*, vol. 56, no. 5, pp. 1411–1419, May 2009.

[4] S. Yim, J. Choi, and K. Yi, "Coordinated control of hybrid 4WD vehicles for enhanced maneuverability and lateral stability," *IEEE Trans. Veh. Technol.*, vol. 61, no. 4, pp. 1946–1950, May 2012.

[5] K. Jalali, T. Uchida, S. Lambert, and J. McPhee, "Development of an advanced torque-vectoring control system for an electric vehicle with in-wheel motors using soft computing techniques," *SAE Int. Alt. Power.*, vol. 2, no. 2, pp. 261–278, Apr. 2013.

[6] D. A. Crolla and D. Cao, "The impact of hybrid and electric powertrains on vehicle dynamics, control systems and energy recuperation," *Veh. Syst. Dyn.*, vol. 50, no. S1, pp. 95–109, Jan. 2012.

[7] D. Akaho, "Development of vehicle dynamics control system for in-wheel-motor vehicle," presented at the JSAE Annual Autumn Congr., Nagoya, Japan, 2010, 120-10.

[8] K. Shimada and Y. Shibahata, "Comparison of three active chassis control methods for stabilizing yaw moments," presented at the Int. Congr. Expo., Detroit, MI, USA, 1994, SAE Tech. Paper 940870.

[9] Y. Shibahata, K. Shimada, and T. Tomari, "Improvement of vehicle maneuverability by direct yaw moment control," *Veh. Syst. Dyn.*, vol. 22, no. 5/6, pp. 465–481, Jan. 1993.

[10] L. De Novellis, A. Sorniotti, and P. Gruber, "Optimal wheel torque distribution for a four-wheel-drive fully electric vehicle," *SAE Int. J. Passenger Cars—Mech. Syst.*, vol. 6, no. 1, pp. 128–136, Apr. 2013.

[11] E. K. Liebemann, K. Meder, J. Schuh, and G. Nenninger, "Safety and performance enhancement: The Bosch Electronic Stability Control (ESP)," presented at the Int. Congr. Expo., Transp. Electron., Detroit, MI, USA, 2004, SAE Tech. Paper 2004-21-0060.

[12] J. Wang and R. G. Longoria, "Coordinated and reconfigurable vehicle dynamics control," *IEEE Trans. Control Syst. Technol.*, vol. 17, no. 3, pp. 723–732, May 2009.

[13] M. Canale, L. Fagiano, A. Ferrara, and C. Vecchio, "Vehicle yaw control via second-order sliding-mode technique," *IEEE Trans. Ind. Electron.*, vol. 55, no. 11, pp. 3908–3916, Nov. 2005.

[14] S. Zheng, H. Tang, Z. Han, and Y. Zhang, "Controller design for vehicle stability enhancement," *Control Eng. Pract.*, vol. 14, no. 12, pp. 1413–1421, Dec. 2006.

[15] C. Poussot-Vassala, O. Senameb, L. Dugardb, and S. M. Savaresi, "Vehicle dynamic stability improvements through gain-scheduled steering and braking control," *Veh. Syst. Dyn.*, vol. 49, no. 10, pp. 1576–1621, Oct. 2011.

[16] L. De Novellis, A. Sorniotti, and P. Gruber, "Wheel torque distribution criteria for electric vehicles with torque-vectoring differentials," *IEEE Trans. Veh. Technol.*, vol. 63, no. 4, pp. 1593–1602, May 2014.

[17] L. De Novellis, A. Sorniotti, P. Gruber, and A. Pennycott, "Comparison of feedback control techniques for torque-vectoring control of fully electric vehicles," *IEEE Trans. Veh. Technol.*, vol. 63, no. 8, pp. 3612–3623, Oct. 2014.

[18] Y. Chen and J. Wang, "Adaptive energy-efficient control allocation for planar motion control of over-actuated electric ground vehicles," *IEEE Trans. Control Syst. Technol.*, vol. 22, no. 4, pp. 1362–1373, Jul. 2014.

[19] V. Utkin, J. Guldner, and J. Shi, *Sliding Mode Control in Electromechanical Systems*. New York, NY, USA: Taylor & Francis, 1999.

[20] A. Levant and L. Alelishvili, "Integral high-order sliding modes," *IEEE Trans. Autom. Control*, vol. 52, no. 7, pp. 1278–1282, Jul. 2007.

[21] E. Bakker, L. Nyborg, and H. Pacejka, "Tyre modelling for use in vehicle dynamics studies," presented at the SAE Int. Conf., Warrendale, PA, USA, 1987, SAE Tech. Paper 870421.

[22] S. Murata, "Innovation by in-wheel-motor drive unit," *Veh. Syst. Dyn.*, vol. 50, no. 6, pp. 807–830, Jun. 2012.

[23] N. Amann, J. Bocker, and F. Prenner, "Active damping of drive train oscillations for an electrically driven vehicle," *IEEE/ASME Trans. Mechatronics*, vol. 9, no. 4, pp. 697–700, Dec. 2004.

[24] F. Bottiglione, A. Sorniotti, and L. Shead, "The effect of half-shaft torsion dynamics on the performance of a traction control system for electric vehicles," *Proc. IMechE D—J. Autom. Eng.*, vol. 226, no. 9, pp. 1145–1159, Sep. 2012.

[25] A. Amos, "Comparison of event-triggered and time-triggered concepts with regard to distributed control systems," in *Proc. Embedded World Conf.*, 2004, pp. 235–252.

[26] H. Lonn and J. Axelsson, "A comparison of fixed-priority and static cyclic scheduling for distributed automotive control applications," in *Proc. 11th Euromicro Conf. Real-Time Syst.*, 1999, pp. 142–149.

[27] R. Davis, A. Burns, R. Bril, and J. Lukkien, "Controller Area Network (CAN) schedulability analysis: Refuted, revisited and revised," *Real Time Syst.*, vol. 35, no. 3, pp. 239–272, Apr. 2007.

[28] Z. Shuai, H. Zhang, J. Wang, J. Li, and M. Ouyang, "Combined AFS and DYC control of four-wheel-independent-drive electric vehicles over CAN network with time-varying delays," *IEEE Trans. Veh. Technol.*, vol. 63, no. 2, pp. 591–601, Feb. 2014.

[29] Z. Shuai, H. Zhang, J. Wang, J. Li, and M. Ouyang, "Lateral motion control for four-wheel-independent-drive electric vehicles using optimal torque allocation and dynamic message priority scheduling," *Control Eng. Pract.*, vol. 24, pp. 55–66, Mar. 2013.

[30] C. S. Ahn, "Robust estimation of road friction coefficient for vehicle active safety systems," Ph.D. dissertation, Univ. Michigan, Ann Arbor, MI, USA, 2011.
[31] J. Hahn, R. Rajamani, and L. Alexander, "GPS-based real-time identification of tire–road friction coefficient," *IEEE Trans. Control Syst. Technol.*, vol. 10, no. 3, pp. 331–343, May 2002.
[32] G. Baffet, A. Charara, and J. Stephant, "Sideslip angle, lateral tire force and road friction estimation in simulations and experiments," in *Proc. IEEE Int. Symp. Intell. Control*, 2006, pp. 903–908.
[33] Y. Chen and J. Wang, "Vehicle-longitudinal-motion-independent real-time tire–road friction coefficient estimation," in *Proc. 49th IEEE Conf. Decision Control*, 2010, pp. 2910–2915.
[34] J. Tjonnas and T. A. Johansen, "Stabilization of automotive vehicles using active steering and adaptive brake control allocation," *IEEE Trans. Control Syst. Technol.*, vol. 18, no. 3, pp. 545–558, May 2010.
[35] A. Viehweider and Y. Hori, "Electric vehicle lateral dynamics control based on instantaneous cornering stiffness estimation and an efficient allocation scheme," in *Proc. 7th Vienna Int. Conf. Math. Model.*, 2012, pp. 1213–1218.
[36] L. Feiqiang, W. Jun, and L. Zhaodu, "On the vehicle stability control for electric vehicle based on control allocation," in *Proc. IEEE VPPC*, Harbin, China, 2008, pp. 1–6.
[37] R. Limpert, *Brake Design and Safety*. Warrendale, PA, USA: SAE, 1999.
[38] G. Genta, *Motor Vehicle Dynamics: Modeling and Simulation*. Singapore: World Scientific, 1997.
[39] A. Levant, "Chattering analysis," *IEEE Trans. Autom. Control*, vol. 55, no. 6, pp. 1380–1389, Jun. 2010.
[40] I. Boiko, L. Fridman, A. Pisano, and E. Usai, "Analysis of chattering in systems with second order sliding modes," *IEEE Trans. Autom. Control*, vol. 52, no. 11, pp. 2085–2102, Nov. 2007.

Tommaso Goggia received the M.Sc. (*summa cum laude*) degree in computer engineering from the University of Pavia, Pavia, Italy, in 2013. He was also a student of the Almo Collegio Borromeo of Pavia and of the Science and Technology Class of the Institute for Advanced Studies of Pavia.

After a period working as a Research Assistant with the University of Surrey, Guildford, U.K., he is currently a Software Testing Engineer with McLaren Automotive Ltd., Woking, U.K.

Aldo Sorniotti (M'12) received the M.Sc. degree in mechanical engineering and the Ph.D. degree in applied mechanics from Polytechnic University of Turin, Turin, Italy, in 2001 and 2005, respectively.

He is currently a Reader in advanced vehicle engineering with the University of Surrey, Guildford, U.K. He is also the Project Coordinator of E-VECTOORC. His main research interests include vehicle dynamics, control and transmission systems for electric vehicles.

Leonardo De Novellis (M'12) received the M.Sc. degree in mechanical engineering and the Ph.D. degree in mechanical and biomechanical design from the Polytechnic University of Bari, Bari, Italy, in 2006 and 2010, respectively.

Since 2011, he has been a Research Fellow with the University of Surrey, Guildford, U.K. His main research interests include vehicle dynamics control and continuously variable transmissions.

Antonella Ferrara (S'86–M'88–SM'03) received the M.Sc. degree in electronic engineering and the Ph.D. degree in computer science and electronics from the University of Genoa, Genoa, Italy, in 1987 and 1992, respectively.

Since 2005, she has been a Full Professor of automatic control with the University of Pavia, Pavia, Italy. Her main research interests include sliding mode control applied to automotive systems, process control, and robotics.

Dr. Ferrara is a member of the IEEE Technical Committee on Automotive Control and the Chair of the Women in Control Committee.

Patrick Gruber received the M.Sc. degree in motorsport engineering and management from Cranfield University, Bedford, U.K., in 2005 and the Ph.D. degree in mechanical engineering from the University of Surrey, Guildford, U.K., in 2009.

He is currently a Senior Lecturer in advanced vehicle systems engineering with the University of Surrey. His current research interests include tire dynamics and development of novel tire models.

Johan Theunissen received the M.Sc. degree in electromechanical engineering from the Catholic University of Leuven, Leuven, Belgium, in 2007.

He is currently a Senior Researcher and a Team Leader within the Research Department, Flanders' Drive, Lommel, Belgium. His main research interests include the areas of control engineering applied to vehicle powertrains, chassis control systems, and autonomous driving.

Dirk Steenbeke received the M.Sc. degree in electromechanical engineering and industrial business policy from the Catholic University of Leuven, Leuven, Belgium.

He is currently a Research and Development Manager with Flanders' Drive, Lommel, Belgium, where he is responsible for 30 researchers and project managers. In addition to his industrial experience at automotive original equipment manufacturers and in the development of high-voltage systems, he is involved as Project Leader in several Seventh Framework Programme consortia in the area of energy-efficient vehicles.

Bernhard Knauder received the Dipl.-Ing. degree in telematics from Graz University of Technology, Graz, Austria, in 2008.

He is currently a Senior Researcher in the area of electrics/electronics and software with the Virtual Vehicle Research Center, Graz. His main research interests include vehicle control, system optimization, and advanced driver-assistance systems.

Josef Zehetner (M'08) received the M.Sc. degree in telematics and the Ph.D. degree in control science from Graz University of Technology, Graz, Austria, in 2003 and 2008, respectively.

He was the E-VECTOORC Project Manager at the Virtual Vehicle Research Center, Austria. He is currently a Manager for IODP system architecture with AVL List GmbH, Graz. His main research interests include vehicle dynamics, cosimulation and simulation data management.